Special Section: Ground Penetrating Radar in Hydrogeophysics
Vadose Zone Journal

Hydrostratigraphic Characterization of Glaciofluvial Deposits Underlying an Infiltration Basin Using Ground Penetrating Radar

David Goutaland,* Thierry Winiarski, Jean-Sébastien Dubé, Grégory Bièvre, Jean-François Buoncristiani, Michel Chouteau, and Bernard Giroux

An understanding of the heterogeneity of quaternary gravelly deposits is required to predict flow and contaminant transfer through these formations. In such deposits, preferential flow paths can lead to contamination at depths greater than predicted under the assumption of a homogeneous medium. The difficulties in characterizing their complex structure with conventional methods represent an obstacle for this prediction. In this study, we developed an approach relying on the use of ground penetrating radar (GPR) for the detection of sedimentary depositional units. A genetic interpretation of the radar stratigraphy allowed us to construct a distribution model of lithofacies. The study was conducted on glaciofluvial deposits underlying a stormwater infiltration basin. Two main system tracts were characterized: a top stratum (50–80 cm deep) corresponding to massive gravel and open-framework gravel, and a base stratum corresponding to trough-fill structures with associated sandy, open-framework, massive, and matrix-rich gravelly lithofacies. The knowledge of the hydraulic properties linked to each lithofacies led us to propose a hydrostratigraphic model. Based on this model, we formulated a hypothesis about the hydraulic behavior of the deposit during stormwater infiltration. Open-framework gravels can act, during complete saturation, as preferential flow paths, and capillary barrier effects may occur under variably saturated conditions. These hypotheses were tested by measuring water content variations (using time domain reflectometry probes) at three depths (0, −0.5, and −1.15 m). Experimental data show infiltration behavior that can be explained by a capillary barrier effect between the two lower probes. These results suggest that our hypothesis about hydraulic behavior is reasonable.

Abbreviations: BM, bimodal gravels hydrofacies; GPR, ground penetrating radar; M, massive gravels hydrofacies; OW, open-framework gravels hydrofacies; S, sand hydrofacies; TDR, time domain reflectometry.

About 50% of the world's population, about 80% in Europe, lives in urban areas, and this percentage is continuously increasing (Biasioli et al., 2006). This population concentration leads to a great exposure of underground media (subsoil and water resources) to anthropogenic contaminants. Among the natural soils underlying urban areas, quaternary alluvial deposits are widely represented. For example, in southeastern France, 74% of the population is living on surficial alluvial deposits (glaciofluvial and fluvial deposits), which represent 29% of the whole Rhône–Mediterranean catchment area. These deposits form large aquifers, which need to be preserved for their use as a drinking water resource. The vadose zone overlying these aquifers plays a dominant role in contaminant retention mechanisms; however, sedimentary deposits constituting aquifers and vadose zones are complex, three-dimensional, heterogeneous, and commonly anisotropic (Fraser and Davis, 1998). Hydraulic heterogeneities may generate preferential flow paths, leading to contaminant transfer deep in the deposit. These hydraulic heterogeneities are related to the complex nature of the erosion and sedimentation processes that have often resulted in a highly heterogeneous distribution of sedimentary facies. Understanding how sedimentary heterogeneities affect fluid flow and contaminant transfer is thus required for the preservation of underground water resources (Huggenberger and Aigner, 1999; Klingbeil et al., 1999; Bridge and Hyndman, 2004).

The prediction of these mechanisms requires reliable knowledge of the spatial distribution of hydrogeologic properties. Such knowledge cannot be provided by classical investigation techniques like boreholes (which often have wide spacing, making lateral interpolation difficult) or pumping tests (which provide effective parameters at a scale much larger than the typical length of structures in a heterogeneous aquifer; Beres et al., 1999; Klingbeil et al., 1999; Regli et al., 2002, 2003). In recent years, hydrogeophysics has developed to provide quantitative information about subsurface hydrogeologic parameters or processes that can be used as input for flow and transport models (Hubbard and Rubin, 2005).

D. Goutaland and T. Winiarski, Univ. de Lyon, 69003 Lyon, France, Laboratoire des Sciences de l'Environnement, E.N.T.P.E., rue M. Audin, 69518 Vaulx-en-Velin, France; J.-S. Dubé, Dep. Génie de la Construction, Ecole de Technologie Supérieure, 1100 rue Notre-Dame Ouest, Montréal, QC H3C 1K3, Canada; G. Bièvre, Laboratoire de Geophysique Interne et Tectonophysique, UMR CNRS 5559, BP 53, 38041 Grenoble Cedex 9, France, and Laboratoire Régional des Ponts et Chaussées, Boulevard de l'Industrie, B.P. 141, 71404 Autun Cedex, France; J.-F. Buoncristiani, Centre des Sciences de la Terre, UMR CNRS 5561 Biogéosciences, Université de Bourgogne, 6 Bd Gabriel, 21000 Dijon, France; M. Chouteau and B. Giroux, Dep. des Génies Civil, Géologique et des Mines, Ecole Polytechnique de Montréal, C.P. 6079, Succ. Centre-Ville, Montréal, QC H3C 3A7, Canada.
Received 8 Jan. 2007. *Corresponding author (goutaland@entpe.fr or winiarski@entpe.fr).

Vadose Zone J. 7:194–207
doi:10.2136/vzj2007.0003

A first widely used approach in hydrogeophysics consists of direct hydraulic parameter estimation using geophysical measurements and petrophysical relationships, which relate hydrogeologic properties and geophysical attributes. Hubbard and Rubin (2005) listed the most common geophysical methods used for this approach, depending on the estimation objective (e.g., surface and crosshole electrical resitivity tomography, seismic method, surface and cross-hole GPR). Few studies have been performed, however, to improve characterization of the vadose zone. In particular, estimation of the water content in the vadose zone can be performed using GPR (van Overmeeren et al., 1997; Grote et al., 2003; Huisman et al., 2003; Lunt et al., 2005), electrical resistivity (Banton et al., 1997; Yeh et al., 2002), or a combination of both (Dannowski and Yaramanci, 1999). This hydrogeophysical approach often presents the problem of the uncertain and potentially non-unique relation between geophysical and hydrogeologic properties (Hubbard et al., 1997; Hyndman and Tronicke, 2005).

Hubbard and Rubin (2005) defined a second hydrogeophysical approach known as *hydrogeologic mapping*, which infers information about the geometry of subsurface units or interfaces from geophysical measurements. Sedimentological studies provide information about the depositional paleosystem, from which the spatial continuity of stratigraphic units and connected hydrogeological properties across a range of spatial scales can be inferred. As highlighted by Fraser and Davis (1998), sedimentological information is an essential key to solve hydrogeologic problems. Sedimentologists can develop conceptual models that can be used to accurately portray the geometry, boundary characteristics, and heterogeneity of aquifer or vadose zone systems. They can provide more accurate, continuous, and detailed delineation of the geometry of internal sedimentary facies and bedding architecture of hydrostratigraphic units. Known or inferred spatial variation of facies parameters, from direct observations or from geophysical measurements, can then be used as a surrogate for defining the spatial distribution of hydrologic parameters. Moreover, the experience and observations of sedimentologists, notably from modern analogs, are useful in calibrating or adjusting a conceptual model to match the field observations and to provide information that can be used in flow and transport models within aquifers and vadose zones. In this study, we used this second mapping hydrogeophysical approach. To define a reliable three-dimensional hydrostratigraphic model, we extrapolated direct and detailed information about subsurface sedimentology and hydrogeology from less invasive and more laterally continuous geophysical data.

Among the geophysical methods used in the aforementioned type of studies, GPR has been extensively used to study alluvial deposits, notably because of its particular suitability for the characterization of highly resistive sediments, which are mostly composed of sands and gravels (Bristow and Jol, 2003). Several examples of GPR measurements on quaternary deposits show the ability of this hydrogeophysical approach to define three-dimensional hydrostratigraphic models (Huggenberger et al., 1994; Asprion and Aigner, 1999; Beres et al., 1999; Heinz and Aigner, 2003b; Lunt et al., 2004; Kostic et al., 2005; Huggenberger and Regli, 2006).

We studied a glaciofluvial deposit underlying a stormwater infiltration basin. Infiltration basins represent alternative techniques to classical drainage systems, which consist in rapid stormwater evacuation via a sewer network in the direction of the hydrologic network, and strongly modify the natural water cycle. Infiltration basins are frequently used if the hydrologic network is too far away and if the underlying subsoils are highly permeable. In urban areas, this system may concentrate diffused pollution contained in urban runoff water and then endanger the quality of subsoils and water resources. The aim of our study was to assess the impact of a stormwater infiltration system on heterogeneous deposits and underlying aquifers (Barraud et al., 2002; Winiarski et al., 2006).

In our study, we followed an approach similar to that described by Bridge and Hyndman (2004) and used by Lunt et al. (2004) to define a three-dimensional model of a braided river deposit—an approach that can be used as a model for aquifer characterization. Our approach consisted in relating GPR reflection features to sedimentary structures of the glaciofluvial deposit under study. This relation allowed interpretation of the radar stratigraphy and definition of a spatial distribution of lithofacies. Lithofacies were then related to corresponding hydrofacies (i.e., homogeneous, isotropic or anisotropic, sedimentological units hydrogeologically relevant; Anderson, 1989) by assigning them hydraulic properties (in this study, saturated hydraulic conductivity and porosity).

Our work was conducted in four steps, as shown in Fig. 1. First, a sedimentological analysis of the trench walls was performed to describe the glaciofluvial lithofacies, depositional units, and ancient depositional environments corresponding to the studied glaciofluvial deposits. The second step consisted in the calibration of GPR reflections with the sedimentary structures of the trench walls to set up a classification of GPR stratigraphy as a function of lithofacies, depositional units, and system tracts. The third step consisted in a GPR investigation of an area of the infiltration basin for which the sedimentary structure had not been characterized beforehand (i.e., no trench excavation). The classification of GPR stratigraphy was used to interpret GPR reflections. A two-dimensional lithological model was defined. Hydraulic properties were assigned to each lithofacies to propose a hydrostratigraphic model of the glaciofluvial deposit. Finally, this interpretation was compared with water content variations measured using time domain reflectometry (TDR) probes in a measurement well. The probes were placed in a vertical section corresponding to the two-dimensional hydrostratigraphic model to evaluate the compatibility of the hypotheses about hydraulic behavior made from this model with experimental water content measurements.

The purpose of this study was to develop a hydrogeophysical method to define a realistic interpretative model of vadose zone properties by taking into account sedimentary heterogeneities at the lithofacies scale. The definition of this realistic model is an important step toward the successful numerical modeling of unsaturated water flow and transfer in alluvial deposits.

Field Site and Installations

Field Site Description

The field site is a stormwater infiltration basin, named Django Reinhardt basin (DjR basin), located in Chassieu in the eastern suburbs of Lyon, France (Fig. 2), located at northern-

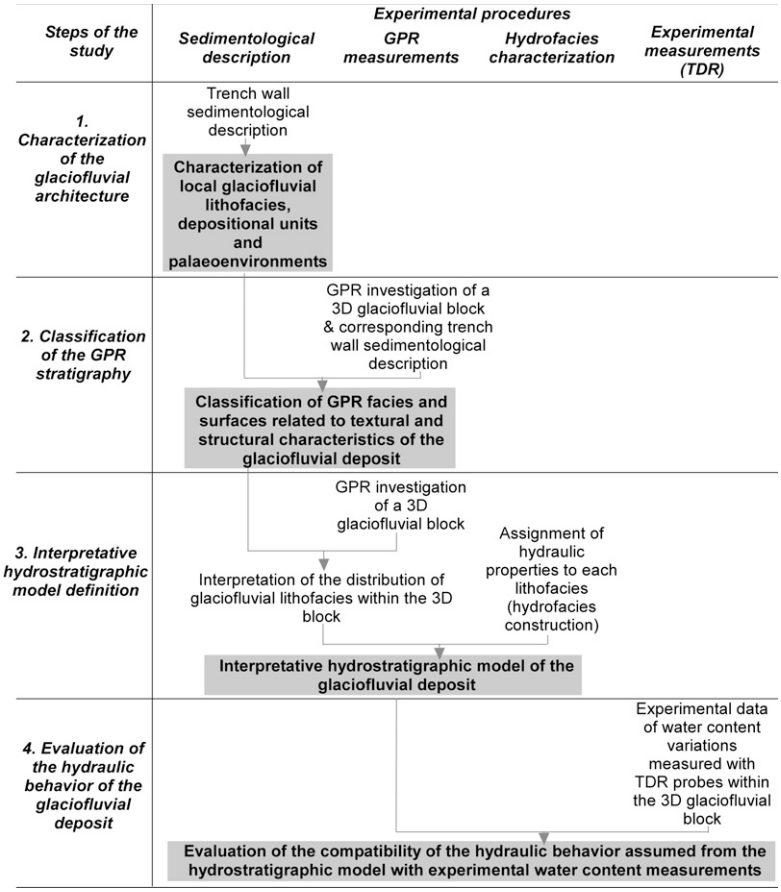

FIG. 1. Workflow for the hydrostratigraphic modeling of glaciofluvial deposits and the evaluation of the coherence of this model. Results expected for each step are in bold and underlined. They are used to interpret the experimental results of the following step (as shown by the arrows).

most 45.8°, southernmost 45.5°, easternmost 3°, westernmost 2.5°. The stormwater catchment corresponds to the industrial area located to the south of Chassieu (185 ha). The basin covers an area of 1 ha. The groundwater level is 13 m below the bottom of the infiltration basin. This basin is downstream of a storage and settling basin. It is located on quaternary deposits of a glaciofluvial corridor (southeast–northwest orientation), deposited during the last glacial maximum (Fig. 2). The thickness of the deposits in this corridor is approximately 30 to 35 m (Barraud et al., 2002). These glaciofluvial sediments rest on an impervious substratum of tertiary mollassic sands. The aquifer has a mean hydraulic conductivity of 7 to 9 × 10^{-3} m s^{-1} (BURGEAP, 1995).

Trench Excavation in the Glaciofluvial Deposit

To perform a sedimentological description of the glaciofluvial deposit, trenches were excavated with a mechanical shovel to expose glaciofluvial sediments. This was done at two locations on the basin (Fig. 3). These trenches were oriented perpendicular to each other to have the longest lateral characterization in two orthogonal sections crossing the proglacial paleoflow orientation. The trench wall located in the northwestern part of the DjR basin, named Section A, was 15 m long and 2.5 m deep. Its orientation was 18° N. The trench wall located in the northeastern part, named Section B, was 15 m long and 3 m deep. Its orientation was 110° N. Only Section A is presented here. Results concerning Section B were presented by Goutaland et al. (2005).

Measurement Well

A concrete-lined measurement well was constructed in 2001 at the bottom of the infiltration basin (Fig. 3) to characterize the effects of the glaciofluvial structures and textures on the unsaturated flows of stormwater through the deposits underlying the basin. Its diameter is 3.20 m wide, and it is 1.70 m deep (Fig. 4). It allows an in situ monitoring of the water content of the glaciofluvial deposits through the use of TDR probes inserted in the deposits at three levels (0, −0.50. and −1.15 m). The subhorizontal pipes in which TDR probes are inserted are 2 m long and their diameter is 80 mm wide. They were drilled using the ODEX method to conserve the sedimentary structures of the deposits (Winiarski et al., 2004).

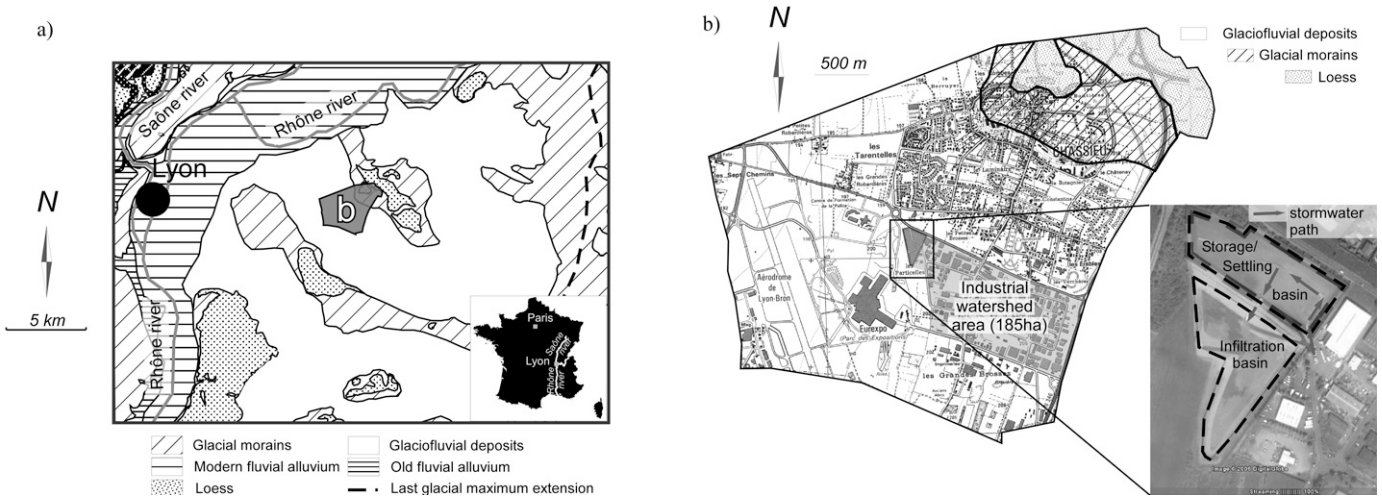

Fig. 2. (a) Geological settings of the eastern part of the Lyon area, and (b) location of the site in the Chassieu city area. The DjR infiltration basin is located in 13-m-deep unsaturated glaciofluvial deposits. It is located downstream from a storage and settling basin.

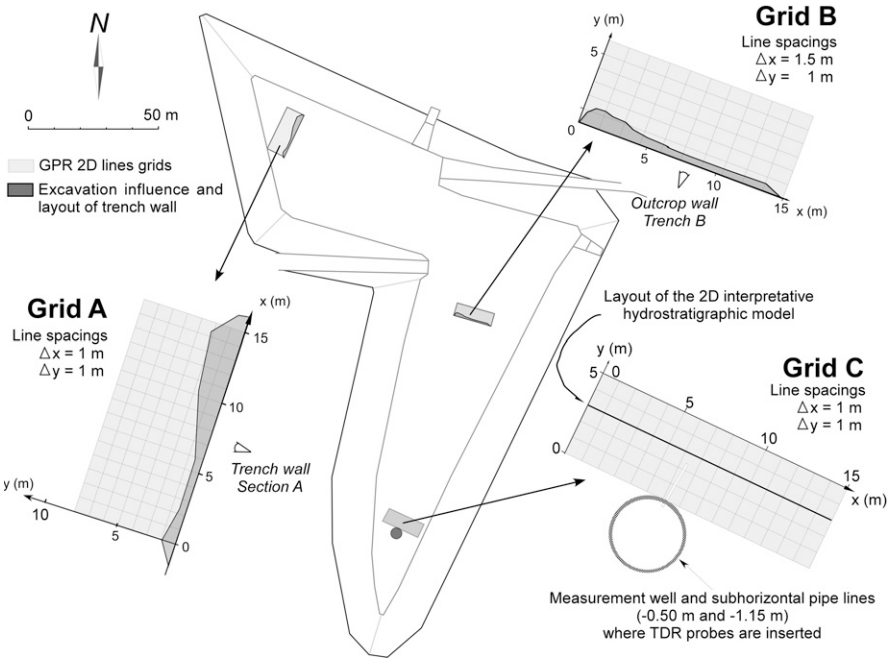

FIG. 3. Measurements performed in the DjR infiltration basin. Ground penetrating radar GPR) reflections calibration was performed from the trench wall excavated on Grid A and Grid B (results are presented by Goutaland et al., 2005). This calibration was used to interpret GPR profiles from Grid C in terms of stratigraphy and hydrostratigraphy. This interpretation was compared with volumetric water content variations at –0.50 and –1.15 m under the basin surface.

Characterization of the Glaciofluvial Sedimentary Architecture

Sedimentological Terminology and Description

A sedimentological description of both trench walls was performed at the textural and structural scales. The textural scale corresponds to sedimentary heterogeneities related to *lithofacies*, which are defined as uniform strata characterized by their distinctive lithological features (composition, grain size, bedding characteristics, and sedimentary structures) and corresponding to an individual depositional event (Miall, 1978). The structural scale is the description scale of the three-dimensional sedimentary bodies, composed of distinctive assemblages of lithofacies and corresponding to the depositional product of a particular process or suite of processes occurring within a depositional system (Miall, 1978). These sedimentary bodies are called *architectural units* or *depositional units* (Heinz et al., 2003). Depositional units are characterized by their internal lithofacies construction, external geometries, and orientation. An understanding of these three-dimensional characteristics enables the reconstruction of ancient fluvial systems (Heinz and Aigner, 2003a). Changes in ancient fluvial system energy corresponds to changes in system tracts. *System tracts* are defined as a linkage of depositional units characterized by common depositional patterns.

Both lithofacies and depositional units of the studied glaciofluvial deposit were characterized. The lithofacies description was performed using the sedimentological code of Miall (1978) extended by Heinz et al. (2003). It allowed us to describe, in the field, lithological units using the main grain size fraction, component fabric (clast- or matrix-supported), sedimentary structures, and other characteristics (Table 1). This description was supplemented by subsequent grain size analysis (NF P94-056 standard, Association Française de Normalisation, 1996) of samples taken on the exposed wall of the trench (86 samples). Changes in lithofacies dip were analyzed to determine the boundaries of depositional units.

Lithofacies Characterization

The four major lithofacies identified in the glaciofluvial sedimentary system are listed in Fig. 5 and are briefly decribed below.

Facies 1: Sandy Lithofacies S-x

This lithofacies is composed of poorly sorted to moderately well sorted medium sands, with a mean grain size of 325 ± 43 μm. No clay or silt matrices are present. Their thickness ranges from a few centimeters to decimeters and their lateral extension ranges from decimeters to meters. Significant sedimentary structures such as planar or low-angle laminations are present. According to Heinz et al. (2003), this lithofacies could correspond to a low-energy deposit occurring in protected areas within the fluvial system. Internal stratification reflects the trans-

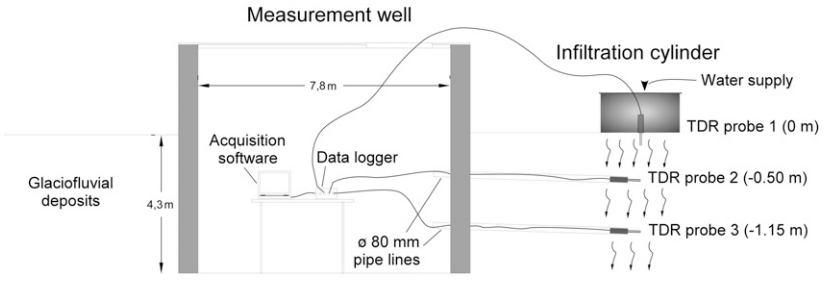

FIG. 4. Schematic presentation of the measurement well constructed in the glaciofluvial deposits underlying the DjR infiltration basin. Time domain reflectometry (TDR) probes at 0, –0.50, and –1.15 m measured volumetric water content variations during water infiltration from the infiltration cylinder. These variations were recorded by the acquisition device located in the measurement well.

TABLE 1. Lithofacies code from Miall (1978) extended by Heinz et al. (2003). This code consists of the juxtaposition of indices I_1, i_2, i_3, and i_4, and defines lithofacies characteristics such as main grain size fraction, component fabric, and sedimentary structure.

Index	Feature	Abbreviation
I_1	main grain size fraction	G, gravel; S, sand
i_2	texture	
	gravel	c, clast-supported; m, matrix-supported
	sand	–, a dash is used to keep the sequence
i_3	sedimentary structure	x, stratified; m, massive (no bedding); g, graded (normal, inverse)
i_4	additional information	o, open framework; b, bimodal

port of single particles as bedload charge (Heinz et al., 2003). This lithofacies could also be formed as migrating dunes in the low-flow regime or as flow waned near the limit of sand bedload transport either on the tops of bars or in emerging chutes along bar flanks (Anderson et al., 1999).

Facies 2 and 3: Massive Gravel and Sand Mixtures Gcm and Gcm,b

These lithofacies are composed of poorly sorted clast-supported massive sands and gravels. The gravel grain size fraction is about 85%. The grain size distribution ranges from fine sands to granules or pebbles. The difference between Gcm and Gcm,b is based on grain size distribution; Gcm has a broader grain size distribution than Gcm,b, whereas Gcm,b grain size distribution is bimodal, with a coarse mode corresponding to the gravel fraction (mainly granules) and a finer moderately well sorted mode corresponding to the sand matrix (mean grain size of about 325 μm). This larger amount of sand matrix in Gcm,b relative to Gcm may be due to a late filling of sand in a gravelly lithofacies (Heinz et al., 2003).

Facies 4: Matrix-Free Lithofacies Gcg,o or Gcx,o

This lithofacies is composed of poorly to moderately well sorted clast-supported gravels without a sandy matrix. Coarser grain size is centimetric and no clay or silt matrices are present. Their thickness ranges from centimeters to decimeters. Their lateral extension ranges from decimeters to meters. Their sedimentary structure is oblique (planar or tangential) or horizontal (base of a gravel sheet).

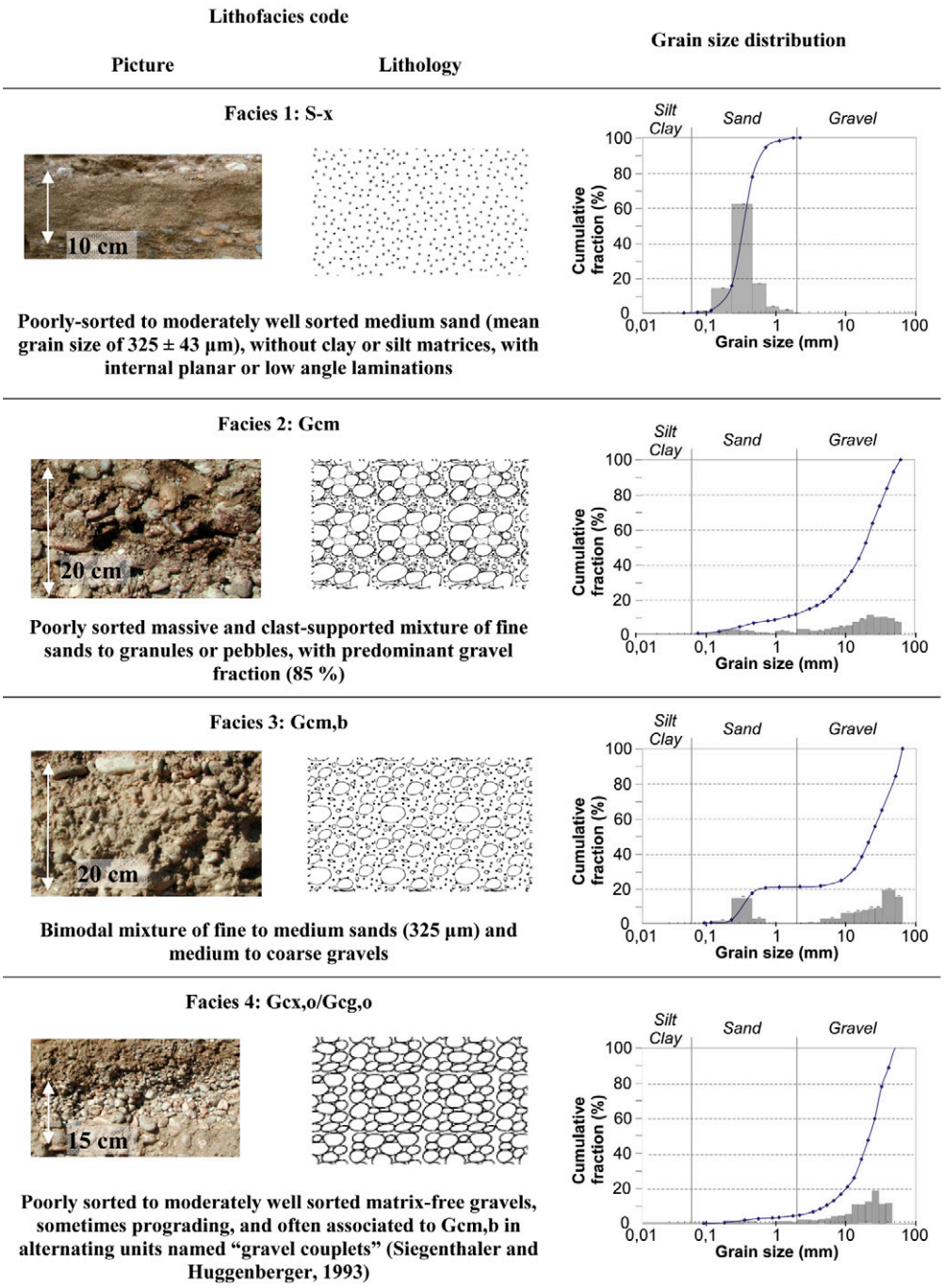

FIG. 5. Lithofacies classification of the glaciofluvial deposits at the field site. Lithofacies code used is the one from Table 1. The glaciofluvial deposits are mainly composed of Gcm and Gcm,b lithofacies.

Matrix-free lithofacies sometimes present a normal grading (Gcg,o). In this case, they are associated with a lower zone composed of Gcm,b lithofacies. This alternating unit has been described in the literature, notably as *gravel couplets* (Siegenthaler and Huggenberger, 1993; Jussel et al., 1994) or *alternating gravel* (Heinz et al., 2003). The Gcm,b–Gcg,o association can be the result of different mechanisms. This alternation could be initiated by negative steps in the glaciofluvial outwash (scour pool or gravel dunes), leading to grain size segregation and turbulence for winnowing or infiltration of the sand matrix in the basal zones (Heinz et al., 2003). Planar strata composed of Gcx,o can be formed by the migration of bedload sheets (Lunt et al., 2004).

Depositional Units

Four depositional units were described on Section A. They are named Units 1, 2, 3, and 4, from the base to the top of the trench wall, corresponding to the basin surface (Fig. 6a).

Unit 1 is present on the northern bottom of the trench wall. It is mainly composed of Gcm and Gcm,b lithofacies in which a fine, matrix-free gravel bed is inserted. This bed slightly dips northward.

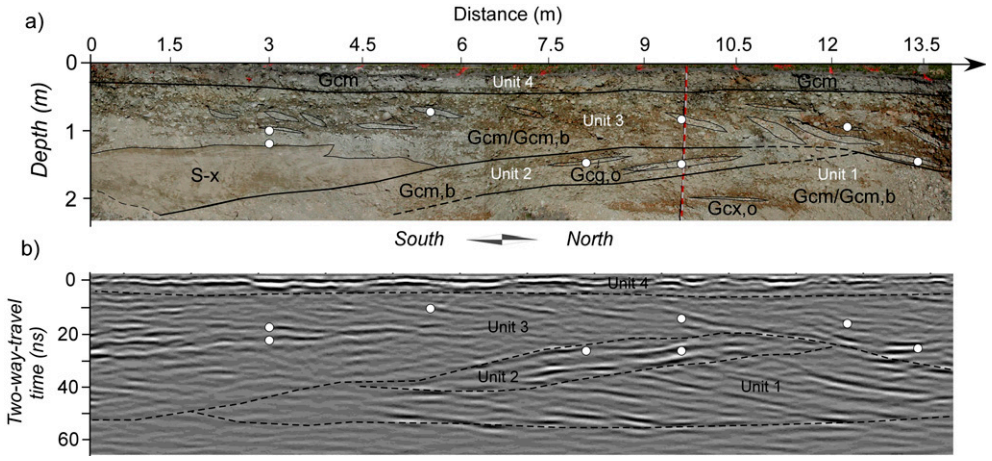

FIG. 6. Comparison of (a) orthonormal picture of Section A, and (b) corresponding GPR profile. Boundaries of depositional units (a and b) and main glaciofluvial lithofacies (a) are outlined. The four lithofacies characterized on the field site are sand and gravel mixtures Gcm and Gcm,b, matrix-free gravels Gcx,o or Gcg,o, and medium sands S-x. Boundaries of depositional units from sedimentological analysis and GPR surfaces correlate well. The eight white points on each figure are the correlation points used to normalize electromagnetic wave velocity, which ranged from 0.094 to 0.111 m ns^{-1} (a mean value of 0.1 m ns^{-1} was chosen).

Unit 2 is composed of an alternation of planar Gcg,o and Gcm,b lithofacies. It corresponds to a dip change as Gcg,o lithofacies dip southward within the Gcm,b lithofacies. The Gcg,o beds have an average thickness of 5 cm.

Unit 3 is made up of a thick, lower S-x lithofacies (1 m at its base) and an upper Gcm lithofacies with intercalated Gcx,o lithofacies. Sedimentary structures in the sand evolve from tangential oblique laminations (dipping northward) at the base to climbing ripples at the top of the sandy layer. These sedimentary structures could be due to an overflow from a paleochannel located in a southerly direction. Northward-dipping Gcx,o lithofacies within the upper Gcm lithofacies confirms the hypothesis of a deposit phase identical to that of the sand.

Unit 4, located just beneath the basin surface, has a thickness of about 25 to 30 cm. This unit seems to have been deposited in a high-energy braided river system, according to the wide grain size distribution of its Gcm lithofacies in which Gcx,o beds are intercalated. This unit is disturbed by the roots of vegetation present at the surface of the basin.

Goutaland et al. (2005) provided a sedimentological description of Section B, where three depositional units were identified: a lower prograding unit of Gcm,b and Gcg,o lithofacies alternation below 2 m, an intermediate trough-fill sequence with associated S-x, Gcg,o, and Gcm,b lithofacies between depths of 0.7 and 2 m, and an upper unit composed of lithofacies Gcm with some inserted Gcx,o fine beds and a greater silt grain size at its base.

System Tracts

The sedimentary environment of the studied glaciofluvial deposit can be divided into two system tracts corresponding to the genesis of the deposit. At the base, we observed depositional units linked to a braided-stream paleoenvironment with dominant trough-fill sedimentation. These "cut-and-fill" structures, described by Heinz et al. (2003) in the Rhine valley, are mainly composed of sands and gravels. Lithofacies described are Gcm, Gcm,b, Gcx,o, Gcg,o, and S-x. The base boundary was not detected.

The upper level (Unit 4 in Fig. 6) corresponds to a high-flow system according to the wide grain size distribution of the Gcm lithofacies, in which some Gcx,o beds are inserted. This upper structure is present in both trench walls. This high-energy system could be an allocyclic event, explaining why the upper structure is present on both trench walls and probably beneath the whole area of the basin.

An interpretation of the tangential dipping Gcm,b–Gcg,o alternation (observed in the northern part of Unit 3) was given by Huggenberger and Regli (2006). This alternation developed simultaneously with the overlying gravel sheet (Unit 4). During the depositional process, the abrupt decrease in topology from a gravel sheet into a trough-shaped structure may have produced a flow separation zone, which would have favored sediment sorting and the development of gravel couplets. Tangential sets of alternating Gcm,b–Gcg,o lithofacies may be explained by gravel dune migration across lateral trough walls.

Finally, the upper horizon corresponds to the root zone of the vegetation present on the surface of the infiltration basin. This level presents a greater amount of silt particles likely to increase high-amplitude GPR reflections under dry conditions (van Dam et al., 2002).

Relating Radar Stratigraphy to Glaciofluvial Architecture

GPR Measurements, Processing, and Interpretation

The GPR measurements presented here were performed with a GSSI (Geophysical Survey System Inc., Salem, NH) SIR 3000 system. We used shielded antennae operating in a monostatic mode (i.e., zero-offset method). At our site, previous GPR investigations at 200, 400, and 900 MHz had been performed and compared to trench walls (Goutaland et al., 2005). These data were used to explore the ability to detect the sedimentary structure at the scale of the required model resolution (i.e., at the lithofacies scale) and the penetration depth for each antenna. The best tradeoff between high resolution and adequate penetration depth was obtained with the 400-MHz antenna. Thus, only results obtained using the 400-MHz antenna are presented here.

All GPR measurements were performed in the unsaturated zone of the basin (the water table is located 13 m below the surface). We translated two-way travel times (in nanoseconds) to actual depth (in meters) by direct calibration of GPR profiles on trench walls: we correlated characteristic GPR reflections with sedimentary interfaces (Fig. 6). Although such calibrations are time dependant (Lunt et al., 2005), the time period during which GPR surveys and trench excavations were performed (<24 h) was short enough to assume that water content and electromagnetic

(EM) wave velocity remained constant during the studies. The evaluation of EM wave velocities ranged from 0.094 to 0.111 m ns^{-1}, with a mean value of 0.102 m ns^{-1}. We used a velocity value of 0.1 m ns^{-1} to convert the radar profiles, recorded in travel time, into depth profiles. This value is similar to estimated velocities measured by common midpoint analysis within the unsaturated zone of analogous quaternary deposits (Beres et al., 1999; Jakobsen and Overgaard, 2002; Heinz and Aigner, 2003b; Kostic et al., 2005). The time range used in this survey provides good quality data up to 80-ns two-way travel time, allowing an investigation depth >4 m. The highest vertical resolution that could be theoretically achieved is one-quarter of the wavelength, λ, of the received dominant frequency, which is about 260 MHz in our case. This theoretical resolution is about 10 cm. In practice, we considered a vertical resolution between $\lambda/2$ and $\lambda/3$ according to Beres and Haeni (1991). Therefore, the vertical resolution was determined to be in the range 12 to 20 cm.

Data acquisition was performed on two grids of orthogonal two-dimensional GPR lines (Fig. 3). One outline of each grid approximately corresponds to the layout of a trench wall. The acquisition grids associated with Sections A and B were named Grid A and B, respectively. Grid A was 15 m north–south by 7 m west–east, with line spacing of 1 m in each direction. Results obtained on Grid B were presented in Goutaland et al. (2005).

Data were collected in common-offset mode by using a constant 30 scans s^{-1} acquisition rate. A bandpass filter was applied; upper and lower cutoff frequencies were 100 and 800 MHz, respectively. A marker was set at each meter. Data processing was performed using the GSSI software Radan 6.5. Distance normalization was performed from markers, with a trace spacing of 40 scans m^{-1}. A static time shift was used to obtain zero-offset traces, i.e., to align the direct ground wave arrival with a two-way travel time equal to 0 ns. A two-dimensional constant-velocity Kirchoff migration was performed using a constant wave velocity evaluated at 0.1 m ns^{-1}. A background removal filter was used to eliminate the high-amplitude direct ground wave. As no other horizontal reflections due to real sedimentary contrasts were present on the profiles, the background removal was defined for all of the samples of the traces. All GPR profiles shown here were processed using the above sequence. In addition, we computed the instantaneous phase to emphasize the continuity of events. This attribute is commonly used in seismic processing (Yilmaz, 1987) to make weak coherent events more prominent. Although this processing helped us to define radar surfaces, GPR profiles processed with the instantaneous phase are not shown here due to space constraints.

Interpretation was performed using the terminology proposed by Neal (2004). This terminology distinguishes *radar facies* (shape, dip, continuity, and the relationship between reflections), *radar surfaces* (reflection geometries), and *radar packages* (three-dimensional external form). Three-dimensional mapping of depositional units was performed by outlining radar surfaces from profile to profile on each grid and by a horizontal interpolation between each profile. This interpolation was performed by kriging the radar surface. Kriging was chosen due to its flexibility in taking into account the spatial anisotropy of the sedimentary structure. We fitted each experimental variogram with an anisotropic linear model with a nugget effect (unless otherwise stated). Azimuths corresponding to the longest correlation length are reported below.

Calibration of GPR Reflections

The GPR reflections were calibrated in two different ways. First, a direct comparison between sedimentological description of the trench wall and corresponding two-dimensional GPR stratigraphy was performed to correlate reflection patterns with glaciofluvial lithofacies and depositional units. Second, an indirect calibration from adjacent trench wall profiles, sampled on grids of orthogonal GPR lines, allowed us to reconstruct the three-dimensional architecture of the depositional units as well as to relate lithofacies and reflection types to a depositional environment.

Figure 6 shows the direct comparison between the orthonormal picture of Section A and the corresponding GPR profile. The analysis of the GPR pattern, surface, and facies (in the sense of Neal [2004]), allows us to distinguish four different units that are well correlated with the four sedimentary depositional units described above.

Unit 1 presents continuous parallel reflections dipping northward and overlapping the lower boundary. They correspond to an alternation of Gcg,o and Gcm,b lithofacies. Only one Gcg,o lithofacies in the sandy-gravelly lithofacies was described during the sedimentological description. The GPR results provided us a better characterization of the sedimentary structure within Unit 1.

The boundaries of Unit 2 were observed with the GPR. This unit is characterized by high-amplitude subparallel reflections, dipping toward the south and concordant with the lower boundary. These reflections are related to the Gcg,o and Gcm,b alternance.

Unit 3 is characterized at depths between 0.3 and 1 m by subparallel reflections dipping northward, with occasional concave reflections at the base of the unit (near a distance of 12 m in the profile). These reflections correspond to the alternating Gcx,o and Gcm,b progradation. On the southern side, similarly dipping reflections are present between 1 and 2 m. Small subhorizontal or slightly oblique reflections are present at the same level. Oblique reflections are due to the sandy laminations. The boundary between sand and upper gravelly lithofacies is characterized by a continuous sinuous reflection dipping slightly southward. It is not possible, however, to characterize the lithology of the sandy facies.

Unit 4 presents continuous, subhorizontal, and slightly wavy reflections. Small wavelets are due to topography variations. Reflections are concordant with the lower boundary. This radar facies is present near the basin surface. The high amplitude of the reflections could be due to a greater quantity of silt particles. Reflections correspond to the Gcm gravels and sands mixture, in which fine Gcx,o gravel beds are inserted.

Characterization of the Depositional System

Figure 7 shows the interpretation of the pseudo-three-dimensional GPR block corresponding to Grid A. The profiles of Grid A near the trench wall were interpreted from the direct calibration on the trench wall. The interpreted radar reflection surfaces (hereafter named *radar surfaces*) are drawn in three dimensions.

Unit 1 presents anisotropy having its longest range oriented at 153° N. This unit presents a trough shape dipping 2.4° to the northeast. Progradations within this unit are oriented northward (10° dip). These progradations may be due to the migration of a gravel dune.

Small Unit 2 has its longest range oriented at 172° N. A horizontal slice at a depth of 1.5 m shows the orientation of this

unit (dark zone on the upper horizontal slice of Fig. 7). This unit has a lens-like external shape and is characterized by high-amplitude reflections corresponding to Gcg,o beds parallel to the unit boundaries (4° southward dip).

Unit 3 has a lower external elongated trough shape characteristic of a paleochannel. The direction of its longest range corresponds to the bottom of the trough shape, i.e., 160° N (orientation of the paleoflow). The northern side presents a 10° northeastward dip, corresponding to the Gcg,o–Gcm,b progradation.

Units 1, 2, and 3 were deposited in a braided system environment. The main orientation of the paleoflow seems to be southeast–northwest. This direction is fully consistent with the glaciofluvial corridor orientation.

The lower boundary of Unit 4 has a rather flat topography (an isotropic linear model was chosen to fit the experimental variogram), except for a north–south-oriented central depression corresponding to an isolated scour structure. The general shape is that of a sheet. Mean depth is about 20 to 30 cm. The base radar surface is an erosive truncation generated during a high-energy event in a braided river system.

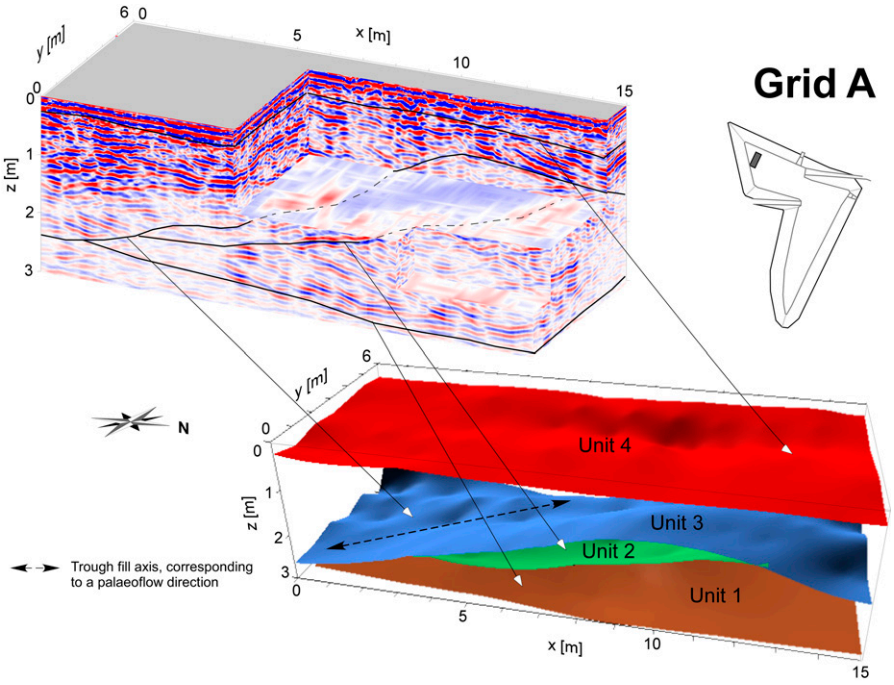

FIG. 7. Ground penetrating radar pseudo-three-dimensional block and three-dimensional interpretation block of depositional units of Grid A. Units 1, 2, and 3 have been deposited in a braided system environment with dominant trough-fill sedimentation. Unit 4 corresponds to a high-energy braided river system.

Classification of Radar Facies

A classification of radar facies was set up from the calibration performed on Section A and the previous results from Section B (Goutaland et al., 2005). The characterization of the three-dimensional architecture of the glaciofluvial deposit was performed following GPR prospecting with the 400-MHz antenna. Three main radar facies (Fig. 8) can be described using the terminology of Neal (2004). This classification is not exhaustive, but shows correlations between Sections A and B. Thus, extrapolations to the whole deposit underlying the basin could be made. Radar facies are listed below:

Radar facies f1: This facies presents laterally continuous, subhorizontal or slightly dipping reflections. They are parallel and concordant with the lower boundary. This radar facies is present near the basin surface, between depths of 0 and 0.50 to 0.80 m (corresponding to two-way travel times of 10–20 ns). It corresponds to the Gcm lithofacies, in which fine Gcx,o beds may be inserted. A greater quantity of fine particles (silts) may contribute to the high-amplitude reflections.

Radar facies f2: This facies is composed of concave or wavy reflections. They are trough cross-stratified. The general organization is a trough form. The reflections correspond to contrasts between minor lithofacies (S-x) with major lithofacies Gcm or Gcm,b. This facies corresponds to trough-fill deposits.

Radar facies f3: This facies presents continuous dipping reflections, subparallel, with occasional cross-cutting between

Code	Reflection features: Reflections	Reflection features: Internal structure	Associated lithofacies	External shape of depositional units (from Neal [2004])	Associated depositional event
f1	high-amplitude, subhorizontal or slightly dip, continous and parallel		Gcm with Gcx,o intercalated	Sheet or wedge shape	High energy event
f2	short, wavy or curved		Mainly Gcm or Gcm,b ; S-x and Gcx,o lenses	Channel shape	Trough structure fill
f3	relatively high-amplitude, oblique, continuous, subparallel, sometimes short and curved		Progradation of Gcg,o / Gcm,b alternation	Trough shape	

FIG. 8. Calibration of GPR reflections with lithofacies organization, depositional units, and depositional events.

reflections. This facies corresponds to progradations of Gcx,o or Gcg,o in sand and gravel mixtures (Gcm, Gcm,b).

Concerning the radar surfaces, contacts between upper units (Unit 1 for Section A) and lower units are erosive truncations due to the erosion of the deposits during a high-energy event. Radar surfaces between lower units are external surfaces of more or less preserved trough structures.

Definition of an Interpretative Hydrostratigraphic Model

The definition of a hydrostratigraphic model of the glaciofluvial deposit was developed from a third GPR survey. This survey was performed on an area for which the sedimentary structures were not characterized by trench excavation. It allowed us to test the classification of the GPR stratigraphy. The model was defined by characterizing the distribution of lithofacies, and then by assigning uniform hydraulic properties (saturated hydraulic conductivity and porosity) to each lithofacies.

Definition of the Lithofacies Distribution

A third grid of two-dimensional orthogonal GPR lines located on the north side of the measurement well was surveyed. This grid, named Grid C, was located perpendicular to the TDR probes (Fig. 3). Data were collected using a GSSI SIR 3000 system with a 400-MHz antenna. The grid area was 15 m west–east by 6 m north–south, with line spacing of 1 m in each direction. Its orientation was 115° N. The processing sequence described above was used. A three-dimensional model of depositional units was proposed. The classification of GPR reflections was used to interpret the radar stratigraphy. A two-dimensional interpretative model of lithofacies distribution was set up, which corresponded to the profile $y = 3$ m of Grid C (in bold in Fig. 3).

Four main depositional units were characterized: Units 5, 6, 7, and 8 from the base to the top of the profile (Fig. 9). Unit 5 is characterized by long continuous reflections dipping westward. They are mainly concave. Unit 6 presents planar oblique high-amplitude reflections dipping eastward. The reflections are long and continuous, parallel to each other. The termination of the reflections overlaps the lower boundary. Unit 7 is characterized by wavy and concave reflections. Reflections are short and discontinuous. The general shape is concave (channel form). The upper unit (Unit 8) is composed of long continuous reflections. They are subhorizontal or dip westward, generally parallel to each other but with some curved reflections. These reflections have high amplitude. Reflections are concordant with the erosive lower radar surface.

The horizontal radar surface interpolation is presented in Fig. 10. Unit 5 presents an intermediate facies between facies f2 and f3, with an inverse dip from that of Unit 6 (westward dip). This unit could be a paleochannel filled on the west side and composed of progradations of Gcm,b–Gcg,o alternation on its eastern side. Unit 6 presents a facies f3. Its external trough shape presents an anisotropy having a longest range direction oriented 0° N and a 9° eastward dip. The internal long dipping reflections are probably due to an alternation between Gcg,o and Gcm,b lithofacies. As explained above, this configuration may be due to gravel dune migration across the lateral trough wall (Huggenberger and Regli, 2006). Unit 7 is characterized by its trough shape, which is oriented 22° N. Internal reflections are characteristic of trough-fill elements (facies f2). Unit 8 has a wedge shape having a longest range oriented 87° N, with a base surface dipping 4° to the northwest. This level presents the characteristics of an f1 facies. Unit 8 may correspond to a succession of high-energy events within a braided river system at the origin of the lower erosive truncation.

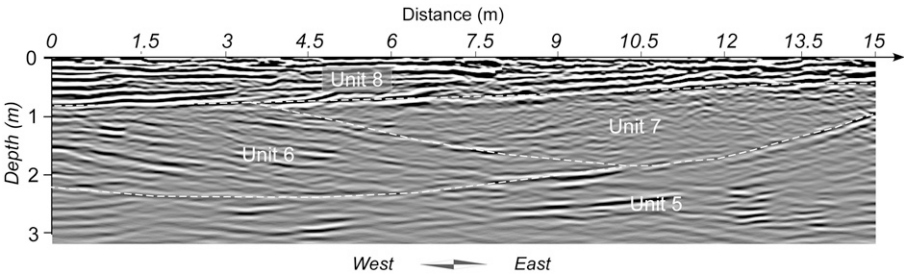

FIG. 9. Ground penetrating radar profile corresponding to the west–east section of Grid C perpendicular to the time domain reflectometry probes of the measurement well. Radar surfaces linked to depositional units are outlined. Four units are characterized: Unit 5, palaeochannel; Unit 6, progradation of an alternation of sand and gravel mixture Gcm,b and matrix-free gravel Gcg,o; Unit 7, trough fill; Unit 8, high-energy deposit.

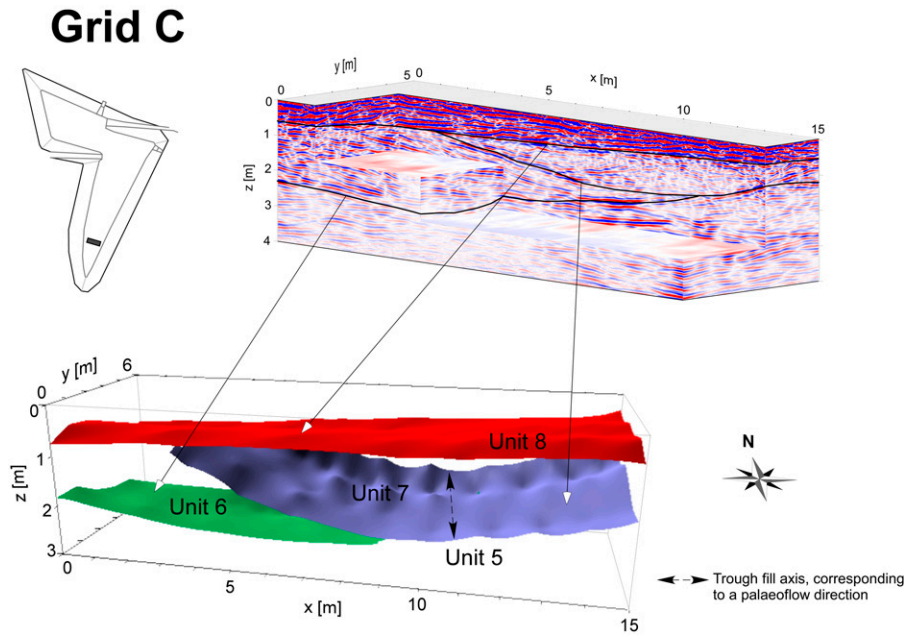

FIG. 10. Ground penetrating radar pseudo-three-dimensional block and three-dimensional interpretation block of depositional units of Grid C. Under the upper unit (high-energy braided river deposit), the boundaries of depositional units are characteristic of a braided system environment (trough-fill unit, progradation of gravelly units).

This unit could be composed of Gcm lithofacies in which some Gcx,o beds are inserted. The contrast between both lithofacies may be at the origin of high-amplitude reflections. A greater amount of fine particles corroborates these high-amplitude reflections. The Gcx,o lithofacies may have a centimetric thickness and a long lateral extension (as in the upper unit of Section B as described by Goutaland et al. [2005]). They may have a westward dip as observed for the radar reflections.

The interpretation of the glaciofluvial stratigraphy underlying Grid C is proposed in Fig. 11a. This two-dimensional interpretative model corresponds to the west–east section perpendicular to the TDR probes.

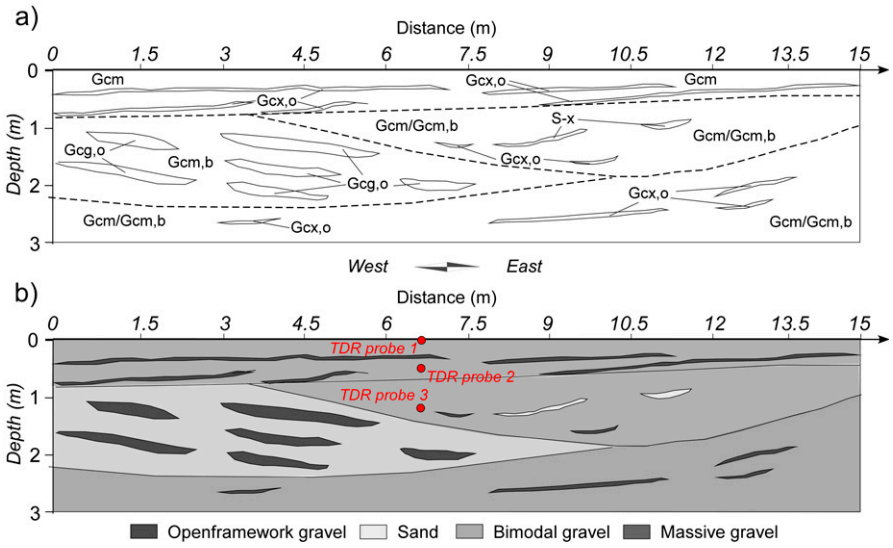

FIG. 11. (a) Lithofacies distribution model drawn from the genetic interpretation of the pseudo-three-dimensional GPR block of Fig. 9, and (b) corresponding hydrostratigraphic model using the lithofacies/hydrofacies relations of Table 2. These interpretative models show an interpretation of the two-dimensional section perpendicular to the time domain reflectometry probes positioned at the end of the pipes.

Lithofacies–Hydrofacies Relation

To define the hydrostratigraphic model, we associated porosity and saturated hydraulic conductivity (K_s) values with the lithofacies of the stratigraphic model of Fig. 11a. We defined *hydrofacies* as hydrogeological units corresponding to lithofacies, and for which uniform hydraulic properties were defined. We associated with each lithofacies the mean porosity values of analogous glaciofluvial lithofacies described in the literature using the same sedimentological code as the one in Table 1 (Jussel et al., 1994; Anderson et al., 1999; Bersezio et al., 1999; Klingbeil et al., 1999; Heinz et al., 2003; Kostic et al., 2005). Porosity values are reported in Table 2. The K_s values were estimated from the Kozeny–Carman expression described in Chapuis and Aubertin (2003). This equation requires lithofacies grain size distribution and void ratio. We used the grain size distributions shown in Fig. 5. Void ratios were calculated from the porosities given in Table 2. The Kozeny–Carman expression is

$$K_s = C\frac{g}{\mu_w \rho_w}\frac{e^3}{S^2 D_R^2 (1+e)}$$

where e is the void ratio, S the specific surface, g is the gravitational constant, μ_w is the dynamic viscosity of water, ρ_w is the density of water, D_R is the specific weight of solids defined as $D_R = \rho_s/\rho_w$ with ρ_s the density of solids (2.65 g cm^{-3}), and C is a constant factor taking into account the shape and tortuosity.

Chapuis and Aubertin (2003) gave the following expression for the specific surface S:

$$S = \frac{6}{\rho_s}\sum\left(\frac{P_{NoD} - P_{Nod}}{d}\right)$$

where $(P_{NoD} - P_{Nod})$ is the percentage by weight smaller than size D (P_{NoD}) and larger than the next size d (P_{Nod}). The sum is performed from a minimum equivalent size d_{eq} corresponding to the mean size of the particles finer than the minimum measured particle size D_{min}:

$$d_{eq}^2 = \frac{1}{D_{min}}\int_0^{D_{min}} y^2 dy = \frac{D_{min}^2}{3}$$

Calculated K_s values associated with each lithofacies are reported in Table 2. We reported also in this table the K_s values proposed in the literature for analogous glaciofluvial lithofacies (Jussel et al., 1994; Anderson et al., 1999; Bersezio et al., 1999; Klingbeil et al., 1999; Heinz et al., 2003; Kostic et al., 2005). The hydrofacies code used in Table 2 is the one proposed by Klingbeil et al. (1999), which distinguished five facies of hydrogeological significance: bimodal gravels (BM); open-framework gravels (OW); planar, trough, and horizontal gravels (P/T/H); massive gravels (M); and sands (S). Figure 11b presents the hydrostratigraphic model resulting from the lithofacies distribution model and the estimated hydraulic properties of Table 2.

Saturated hydraulic conductivity values vary over several orders of magnitude, from

TABLE 2. Hydrofacies characteristics (saturated hydraulic conductivity, K_s, and porosity) of the glaciofluvial deposits underlying the DjR infiltration basin. Calculated K_s values for each hydrofacies were obtained from Fig. 5 with the Kozeny–Carman expression proposed by Chapuis and Aubertin (2003). Data from the literature were obtained from Jussel et al. (1994) (hydrofacies M, S, and OW), Anderson et al. (1999) (M, S, and OW), Bersezio et al. (1999) (M and S), Klingbeil et al. (1999) (M, S, OW, and BM), Heinz et al. (2003) (M, S, OW, and BM), and Kostic et al. (2005) (M, S, OW, and BM).

Hydrofacies code†	Lithofacies‡	Calculated		Data from the literature	
		Mean sand content	K_s	K_s	Porosity experimental values
		%	m s^{-1}	m s^{-1}	%
M	Gcm	14.8 ± 4.2	7.5×10^{-3}	$9.67 \times 10^{-4} \pm 1.36 \times 10^{-3}$	0.24 ± 0.12
BM	Gcm,b	17.4 ± 4.5	1.8×10^{-3}	$2.37 \times 10^{-4} \pm 2.73 \times 10^{-4}$	0.26 ± 0.05
OW	Gcx,o and Gcg,o	7.1 ± 2.5	9.0×10^{-2}	$1.34 \times 10^{-1} \pm 1.46 \times 10^{-1}$	0.30 ± 0.06
S	S-x	97.2 ± 3.7	7.0×10^{-4}	$6.50 \times 10^{-4} \pm 8.09 \times 10^{-4}$	0.31 ± 0.07

† M, massive gravels; BM, bimodal gravels; OW, open-framework gravels; S, sand.
‡ Gcm and Gcm,b are sand and gravel mixtures; Gcx,o and Gcg,o are matrix-free gravels; S-x is medium sand.

mean values of about 10^{-4} m s^{-1} for sandy and bimodal lithofacies (BM and S hydrofacies) to mean values of 10^{-1} m s^{-1} for open-framework matrix-free gravels (OW hydrofacies). Calculated K_s values are in agreement with literature values.

Matrix-free open-framework gravels have the highest K_s. Under fully saturated conditions, their hydraulic conductivity is at least two orders of magnitude higher than that of other glaciofluvial lithofacies. Thus, they may act as preferential flow paths during stormwater infiltration. These fast flow paths can convey dissolved or colloid-bound contaminants. Under unsaturated conditions, the coarse grain size of these gravels may be at the origin of capillary barrier effects at the contact of sand matrix lithofacies, causing water ponding above them (Kowalsky et al., 2004). Therefore, lithofacies located just above the OW hydrofacies can remain in contact with pollutants contained in stormwater for long periods and thus be more exposed to contamination. Carbonated lithofacies, for instance, are known to retain significant amounts of Pb, Cd, and Zn (Plassard et al., 2000).

Comparison between M and BM hydrofacies shows that the sand matrix fraction is a determinant parameter in the control of hydraulic conductivity. Saturated hydraulic conductivities of bimodal and sandy hydrofacies are similar. Massive hydrofacies have a greater saturated hydraulic conductivity. At low suction, we can suppose that, due to their finer mean grain size, BM hydrofacies will be more conductive to water flow than M hydrofacies.

Sandy lithofacies represent, with bimodal lithofacies, the least conductive hydrofacies under fully saturated conditions. Their fine grain size, in comparison with the three other hydrofacies, can lead to a higher degree of saturation under variably saturated conditions. They are, therefore, more exposed to contamination: dissolved contaminants can have a longer residence time in these hydrofacies, and retention mechanisms may have a greater probability of occurrence.

Under fully saturated conditions, OW hydrofacies may act as preferential flow paths. Under transient conditions, hydrofacies with a sandy matrix (M and BM) and sandy hydrofacies (S) may be more conductive than OW hydrofacies. Capillary barriers may develop and cause water ponding above OW hydrofacies, leading to a greater exposure of glaciofluvial deposits to contaminants.

Evaluation of Presumed Hydraulic Behavior from Hydrostratigraphic Model

Infiltration Experiments

Two infiltration tests were performed on the north side of the measurement well to permit the comparison of water content measurements with time as a function of the interpreted hydrostratigraphic model. Each test consisted of a constant-head infiltration of water from a 1-m-diameter cylinder. This cylinder was placed perpendicular to the TDR probes measuring volumetric water content variations at 0 (surface), −0.5, and −1.15 m (Fig. 4). Water supply was maintained by holding a constant water head of 0.20 m for 30 min. The two tests differed in the initial water content of the deposits. The first infiltration test (Infiltration Test A) was performed under initially drier conditions at −1.15 m than the second infiltration test (Infiltration Test B). More details concerning the infiltration tests were described by Winiarski et al. (2004). Qualitative evolution of the water content at both depths was analyzed and interpreted from the assumptions about the hydraulic behavior of the deposits formulated from the hydrostratigraphic model to evaluate the coherence of the interpretative model with respect to experimental field data.

Hydraulic Behavior of the Glaciofluvial Deposit

Figure 12 shows the water content variations at the surface (TDR Probe 1), at −0.50 m (TDR Probe 2), and −1.15 m (TDR Probe 3) during Infiltration Test A (Fig. 12a) and Infiltration Test B (Fig. 12b). Figure 11b shows the location of the three probes on the hydrostratigraphic model. Probe 2 is placed in the upper part (high-energy deposit), dominated by Gcm lithofacies (M hydrofacies) in which Gcx,o lithofacies (OW hydrofacies) are

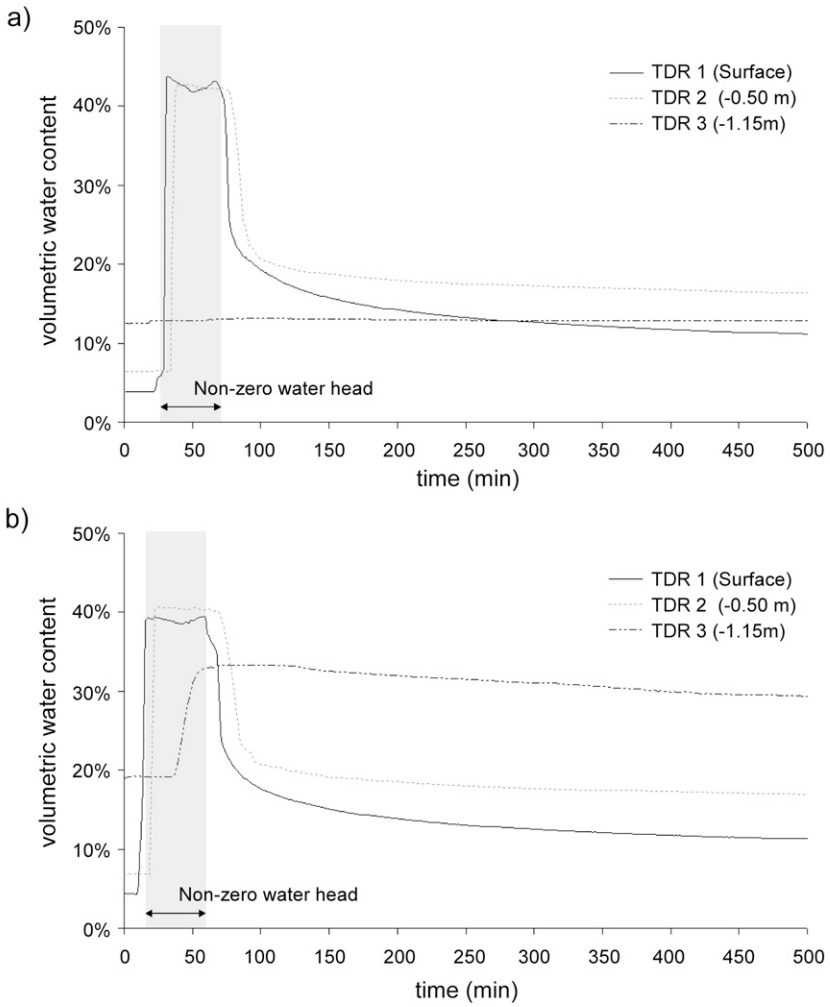

FIG. 12. Volumetric water content variations at the surface (time domain reflectometry [TDR] probe 1), −0.50 m (TDR probe 2), and −1.15 m (TDR probe 3) below the surface of the infiltration basin during (a) Infiltration Test a (initial "dry" conditions at −1.15 m), and (b) Infiltration Test b (initial "humid" conditions at −1.15 m).

inserted according to the interpretative model. Probe 3 is located in the lower level, corresponding to trough-fill deposits.

First, both Fig. 12a and 12b show that water content behavior differed among the three levels. Initial measurements showed similar volumetric water content, θ, for both infiltration tests at the surface (Test A: θ = 3.9%; Test B: θ = 4.4%) and −0.50 m (Test A: θ = 6.4%; Test B: θ = 6.7%). Only the initial water content measured with TDR Probe 3 at −1.15 m significantly differed between the infiltration tests (Test A: θ = 12.5%; Test B: θ = 19.2%).

During the infiltration phase of Test A (infiltration with initially "dry" conditions), volumetric water content reached values between 41.8 and 43.8% at the surface of the basin (TDR Probe 1). The elapsed time corresponding to these values is the time of constant hydraulic head imposition at the surface. The water infiltration began at 29 min. A significant increase in water content was observed at 35 min at TDR Probe 2. This increase corresponds to the appearance of the infiltration front at −0.50 m, with a delay of 6 min with respect to the beginning of water infiltration. No significant increase was measured at −1.15 m. Measured values ranged initially between 12.5 and 13%.

During Infiltration Test B (infiltration with initially "humid" conditions), similar water content variations were measured at TDR Probes 1 and 2. The delay between the arrival of the infiltration front at TDR Probe 1 and TDR Probe 2 was 7 min 30 s. Concerning the water content variations measured at −1.15 m, a significant increase was observed at 38 min, i.e., 26 min after the beginning of water infiltration. This water content increase was slower than those measured at TDR Probes 1 and 2. Water content reached a stage of 33.3%. The decrease in water content following the end of water infiltration was very slow and quasilinear.

It can be assumed that the significant difference in the water content measurements at −1.15 m for both infiltration tests was due to a capillary barrier effect occurring between −0.50 and −1.15 m. Under initially "humid" conditions, the propagation of the infiltration front at this depth could be due to a larger water conductivity of the lower level than under the initially "dry" conditions. This interpretation is in agreement with the interpretative hydrostratigraphic model, in which the upper level, composed of M hydrofacies, could be less conductive under unsaturated conditions than the S or BM hydrofacies constituting the lower part and having a lower mean grain size.

Measurements at the surface and at −0.50 m show values ranging from 39 to 44%. These values are large for M hydrofacies according to the porosity data of Table 2. At the surface, the presence of a larger sand fraction may explain these differences. At −0.50 m, larger values may be explained by the presence of a sand pack made of glaciofluvial facies sieved at 5 mm at the end of the subhorizontal pipes to improve the contact with the TDR probe. This sieved material may explain an increase in porosity and thus a larger water content than expected with regard to the data of Table 2. Water content variations measured at −1.15 m during Infiltration Test B are in the range of values of S hydrofacies according to the porosity data of Table 2. Thus, water content variations at the three levels seem to be in agreement with the proposed interpretative hydrostratigraphic model.

Our study suggests that stormwater infiltration in the vadose zone of such heterogenous quaternary deposits may be significantly influenced by the sedimentary heterogeneity and the initial water content. This assumption will be validated by a complete hydraulic characterization of each hydrofacies.

Conclusions

This study developed a hydrogeophysical approach for the characterization of the spatial distribution of hydraulic properties in quaternary sedimentary deposits. The use of GPR coupled with a sedimentological description of trench walls allowed us to characterize the three-dimensional shape and the nature of the main depositional units constituting the vadose zone beneath an infiltration basin constructed in glaciofluvial deposits. These deposits are characterized by a braided river sedimentation, leading to trough-fill structures (mainly comprised of sandy or sand-matrix lithofacies) and prograding structures (alternance of open-framework gravels and sandy gravel lithofacies), overlain by a high-energy deposit (comprised of heterometric sandy gravel and some open-framework gravel lithofacies). By providing the main three-dimensional sedimentary characteristics of the glaciofluvial deposits, this approach allowed the definition of a reliable interpretative sedimentary distribution at the lithofacies scale from pseudo-three-dimensional GPR surveys. A relation between lithofacies and hydrofacies allowed us to propose a hydrostratigraphic model of the glaciofluvial deposits. We performed an infiltration experiment to test our assumptions about hydraulic behavior as a function of the interpreted hydrostratigraphic model. This model is coherent with water content variations measured in the vadose zone of the infiltration basin. Open-framework hydrofacies may act as preferential flow paths under saturated conditions, and capillary barrier effects may occur between the two main system tracts.

The use of GPR in this hydrogeophysical approach is promising for the study of the unsaturated water flow mechanisms in underlying subsoils of infiltration basins. The high resolution obtained with the GPR method is suitable for characterization of the geometries of depositional units and dips of the internal lithofacies. Realistic interpretative stratigraphic models may also be defined at the lithofacies scale. Moreover, the vadose zone underlying infiltration basins is often comprised of highly permeable materials without a fine grain size fraction (clays and silts), allowing good penetration depth of radar signals.

To better characterize the impact of stormwater on the heterogeneous vadose zone underneath infiltration basins, a full characterization of hydraulic properties (water retention and hydraulic conductivity curves) is needed. Future research will be focused on the determination of the hydraulic properties of hydrofacies, which can be input into water flow numerical modeling. We showed that analogous glaciofluvial hydrofacies formed in similar depositional systems have similar saturated hydraulic conductivity. Future research has to assess the reliability of evaluating hydraulic properties of hydrofacies on modern analogous glaciofluvial deposits. Indeed, the easy access to the glaciofluvial lithofacies on the surface of these modern analogous deposits (in comparison with the difficulty of accessing quaternary lithofacies by trenching) would allow simple measurement of the hydraulic properties of these lithofacies. The numerical modeling performed from the interpretative hydrostratigraphic model and integrated hydraulic characteristic curves will improve our understanding of unsaturated hydraulic behavior and, therefore, transfer mecha-

nisms in the vadose zone. In particular, this numerical modeling will help us to understand preferential flow mechanisms occurring in the vadose zone of an infiltration basin.

Acknowledgments

We thank the research federation O.T.H.U. for technical support, and the Grand Lyon, Rhône-Alpes region, and the French Ministère de l'Equipement for their financial support. This work was realized in the framework of the 60ème Commission Permanente de Coopération Franco-Québécoise.

References

Anderson, M.P. 1989. Hydrogeologic facies models to delineate large-scale spatial trends in glacial and glaciofluvial sediments. Geol. Soc. Am. Bull. 101:501–511.

Anderson, M.P., J.S. Aiken, E.K. Webb, and D.M. Mickelson. 1999. Sedimentology and hydrogeology of two braided stream deposits. Sediment. Geol. 129:187–199.

Asprion, U., and T. Aigner. 1999. Towards realistic aquifer models: Three-dimensional georadar surveys of Quaternary gravel deltas (Singen Basin, SW Germany). Sediment. Geol. 129:281–297.

Association Française de Normalisation. 1996. Soils: Reconnaissance and tests: Grain size analysis—Standard test method for dry sieving after washing. (In French.) AFNOR Standard NF P94-056. AFNOR, Paris.

Banton, O., M.-K. Seguin, and M.-A. Cimon. 1997. Mapping field-scale physical properties of soil with electrical resistivity. Soil Sci. Soc. Am. J. 61:1010–1017.

Barraud, S., J. Gibert, T. Winiarski, and J.-L. Bertrand Krajewski. 2002. Implementation of a monitoring system to measure impact of stormwater runoff infiltration. Water Sci. Technol. 45:203–210.

Beres, M., and F.P. Haeni. 1991. Application of ground-penetrating-radar methods in hydrogeologic studies. Ground Water 29:375–386.

Beres, M., P. Huggenberger, A.G. Green, and H. Horstmeyer. 1999. Using two- and three-dimensional georadar methods to characterize glaciofluvial architecture. Sediment. Geol. 129:1–24.

Bersezio, R., A. Bini, and M. Giudici. 1999. Effects of sedimentary heterogeneity on groundwater flow in a Quaternary pro-glacial delta environment: Joining facies analysis and numerical modelling. Sediment. Geol. 129:327–344.

Biasioli, M., R. Barberis, and F. Ajmone-Marsan. 2006. The influence of a large city on some soil properties and metals content. Sci. Total Environ. 356:154–164.

Bridge, J.S., and D.W. Hyndman. 2004. Aquifer characterization. SEPM Spec. Publ. 80. Soc. Sediment. Geol., Tulsa, OK.

Bristow, C.S., and H.M. Jol. 2003. Ground penetrating radar in sediments. Geol. Soc. Spec. Publ. 211. Geol. Soc., London.

BURGEAP. 1995. Study of the water table of the eastern part of Lyon area. (In French.) Le Grand Lyon Direction de l'eau, Lyon.

Chapuis, R.P., and M. Aubertin. 2003. On the use of the Kozeny–Carman equation to predict the hydraulic conductivity of soils. Can. Geotech. J. 40:616–628.

Dannowski, G., and U. Yaramanci. 1999. Estimation of water content and porosity using combined radar and geoelectrical measurements. Eur. J. Environ. Eng. Geophys. 4:71–85.

Fraser, G.S., and J.M. Davis. 1998. Hydrogeologic models of sedimentary aquifers. Concepts in Hydrogeol. and Environ. Geol. 1. Soc. Sediment. Geol., Tulsa, OK.

Goutaland, D., T. Winiarski, G. Bièvre, and J.-F. Buoncristiani. 2005. Sedimentological approach interest in stormwater infiltration: Ground penetrating radar characterization. (In French.) Techn. Sci. Methodes 10:71–79.

Grote, K., S. Hubbard, and Y. Rubin. 2003. Field-scale estimation of volumetric water content using ground-penetrating radar ground wave techniques. Water Resour. Res. 39:1321, doi:10.1029/2003WR002045.

Heinz, J., and T. Aigner. 2003a. Hierarchical dynamic stratigraphy in various Quaternary gravel deposits, Rhine glacier area (SW Germany): Implications for hydrostratigraphy. Int. J. Earth Sci. 92:923–938.

Heinz, J., and T. Aigner. 2003b. Three-dimensional GPR analysis of various Quaternary gravel-bed braided river deposits (southwestern Germany). p. 99–110. *In* C.S. Bristow and H.M. Jol (ed.) Ground penetrating radar in sediments. Geol. Soc. Spec. Publ. 211. Geol. Soc., London.

Heinz, J., S. Kleineidam, G. Teutsch, and T. Aigner. 2003. Heterogeneity patterns of Quaternary glaciofluvial gravel bodies (SW-Germany): Application to hydrogeology. Sediment. Geol. 158:1–23.

Hubbard, S.S., and Y. Rubin. 2005. Introduction to hydrogeophysics. p. 3–21. *In* Y. Rubin and S.S. Hubbard (ed.) Hydrogeophysics. Water Sci. Technol. Lib. 50. Springer, Dordrecht, the Netherlands.

Hubbard, S.S., Y. Rubin, and E. Majer. 1997. Ground-penetrating-radar-assisted saturation and permeability estimation in bimodal systems. Water Resour. Res. 33:971–990.

Huggenberger, P., and T. Aigner. 1999. Introduction to the special issue on aquifer-sedimentology: Problems, perspectives and modern approaches. Sediment. Geol. 129:179–186.

Huggenberger, P., E. Meier, and A. Pugin. 1994. Ground-probing radar as a tool for heterogeneity estimation in gravel deposits: Advances in data-processing and facies analysis. J. Appl. Geophys. 31:171–184.

Huggenberger, P., and C. Regli. 2006. A sedimentological model to characterize braided river deposits for hydrogeological applications. p. 51–74. *In* G.H. Sambrook-Smith et al. (ed.) Braided rivers: Process, deposits, ecology, and management. Blackwell Publ., Oxford, UK.

Huisman, J.A., S.S. Hubbard, J.D. Redman, and A.P. Annan. 2003. Measuring soil water content with ground penetrating radar: A review. Vadose Zone J. 2:476–491.

Hyndman, D.W., and J. Tronicke. 2005. Hydrogeophysical case studies at the local scale: The saturated zone. p. 391–412. *In* Y. Rubin and S. Hubbard (ed.) Hydrogeophysics. Water Sci. Technol. Lib. 50. Springer, Dordrecht, the Netherlands.

Jakobsen, P.R., and T. Overgaard. 2002. Georadar facies and glaciotectonic structures in ice marginal deposits, northwest Zealand, Denmark. Quat. Sci. Rev. 21:917–927.

Jussel, P., F. Stauffer, and T. Dracos. 1994. Transport modeling in heterogeneous aquifers: 1. Statistical description and numerical generation of gravel deposits. Water Resour. Res. 30:1803–1817.

Klingbeil, R., S. Kleineidam, U. Asprion, T. Aigner, and G. Teutsch. 1999. Relating lithofacies to hydrofacies: Outcrop-based hydrogeological characterisation of Quaternary gravel deposits. Sediment. Geol. 129:299–310.

Kostic, B., A. Becht, and T. Aigner. 2005. 3-D sedimentary architecture of a Quaternary gravel delta (SW-Germany): Implications for hydrostratigraphy. Sediment. Geol. 181:147–171.

Kowalsky, M.B., Y. Rubin, and P. Dietrich. 2004. The use of ground penetrating radar for characterizing sediments under transient flow conditions. p. 107–127. *In* J.S. Bridge and D.W. Hyndman (ed.) Aquifer characterization. SEPM Spec. Publ. 80. Soc. Sediment. Geol., Tulsa, OK.

Lunt, I.A., J.S. Bridge, and R.S. Tye. 2004. Development of a 3-D depositional model of braided-river gravels and sands to improve aquifer characterization. p. 139–169. *In* J.S. Bridge and D.W. Hyndman (ed.) Aquifer characterization. SEPM Spec. Publ. 80. Soc. Sediment. Geol., Tulsa, OK.

Lunt, I.A., S.S. Hubbard, and Y. Rubin. 2005. Soil moisture content estimation using ground-penetrating radar reflection data. J. Hydrol. 307:254–269.

Miall, A.D. 1978. Lithofacies types and vertical profile models in braided river deposits: A summary. p. 597–604. *In* A.D. Miall (ed.) Fluvial sedimentology. CSPG Mem. 5. Can. Soc. Pet. Geol., Calgary, AB.

Neal, A. 2004. Ground-penetrating radar and its use in sedimentology: Principles, problems and progress. Earth Sci. Rev. 66:261–330.

Plassard, F., T. Winiarski, and M. Petit-Ramel. 2000. Retention and distribution of three heavy metals in a carbonated soil: Comparison between batch and unsaturated column studies. J. Contam. Hydrol. 42:99–111.

Regli, C., P. Huggenberger, and M. Rauber. 2002. Interpretation of drill core and georadar data of coarse gravel deposits. J. Hydrol. 255:234–252.

Regli, C., M. Rauber, and P. Huggenberger. 2003. Analysis of aquifer heterogeneity within a well capture zone, comparison of model data with field experiments: A case study from the River Wiese, Switzerland. Aquat. Sci. 65:111–128.

Siegenthaler, C., and P. Huggenberger. 1993. Pleistocene Rhine gravel: Deposits of a braided river system with dominant pool preservation. p. 147–162. *In* J.L. Best and C.S. Bristow (ed.) Braided rivers. Geol. Soc. Spec. Publ. 75. Geol. Soc., London.

van Dam, R.L., E.H. van den Berg, S. van Heteren, C. Kasse, J.A.M. Kenter, and K. Groen. 2002. Influence of organic matter in soils on radar-wave reflection: Sedimentological implications. J. Sediment. Res. 72:341–352.

van Overmeeren, R.A., S.V. Sariowan, and J.C. Gehrels. 1997. Ground penetrating radar for determining volumetric soil water content: Results of com-

parative measurements at two test sites. J. Hydrol. 197:316–338.
Winiarski, T., J.-P. Bedell, C. Delolme, and Y. Perrodin. 2006. The impact of stormwater on a soil profile in an infiltration basin. Hydrogeol. J. 14:1244–1251.
Winiarski, T., J. Crosnier, S. Vacherie, and B. Métral. 2004. Evaluation of infiltration parameters of the unsaturated zone in an infiltration basin of the eastern part of Lyon area (France). (In French, with English abstract.) p. 1541–1548. *In* Sustainable techniques and strategies in urban water management. Proc. Novatech '2004, Lyon, France. 7–11 June 2004. Groupe de Recherche Rhône-Alpes sur les Infrastructures et l'Eau, Villeurbanne, France.
Yeh, T.-C.J., S. Liu, R.J. Glass, K. Baker, J.R. Brainard, D. Alumbaugh, and D. LaBrecque. 2002. A geostatistically based inverse model for electrical resistivity surveys and its applications to vadose zone hydrology. Water Resour. Res. 38:1278, doi:10.1029/2001WR001204.
Yilmaz, O. 1987. Seismic data processing. Invest. Geophys. 2. Soc. Exploration Geophys., Tulsa, OK.